GCN Analysis of Task-Based fMRI Data for Diagnosis of Schizophrenia

Tejaswini Thota, Reuben Stephen John
School of Computer Science and Engineering, Vellore Institute of Technology, Chennai, India

R Dhanush
School of Electronics Engineering, Vellore Institute of Technology, Chennai, India

Amutha S
School of Computer Science and Engineering, Vellore Institute of Technology, Chennai, India

Heshalini Rajagopal
Department of Electrical and Electronics Engineering, MILA University, 71800 Nilai, Negeri Sembilan, Malaysia

Abstract

This study focuses on schizophrenia, impacting 24 million people globally, characterized by distorted reality and delusions. We propose utilizing a GraphSAGE model and a Graph Convolutional Network (GCN) model on a task-based fMRI data to differentiate schizophrenia instances, with and without auditory-visual hallucinations, utilizing healthy participants for comparison. The study focuses on identifying specific auditory stimuli that can help significantly differentiate individuals experiencing hallucinations. The GraphSAGE model performed better by achieving an accuracy of 97% and 96% on the specified stimuli.

Keywords: Schizophrenia, Hallucination, Graph Convolution, GraphSAGE, fMRI

1. Introduction

Functional Magnetic Resonance Imaging(fMRI) has emerged as a powerful tool in unraveling the intricacies of mental disorders. Among the various types of fMRI, the task-based fMRI serves as an ideal method for understanding the functioning of neurons as it captures real-time brain activity as individuals perform specific cognitive tasks. In the context of schizophrenia, the analysis of task-based fMRI data has proven to provide valuable insights that in turn aid the diagnosis and treatment of this disorder.

Graph Convoluted Network (GCN) is a type of neural network architecture designed to process data structured as graphs. In these graphs, the nodes represent entities, and the edges represent the relationship between the entities. **GCN's** leverage information from the neighboring nodes to perform traditional convolution operations. This methodology is suitable for analyzing fMRI data as they model dynamic changes in brain connectivity. In our investigation, we designate regions of interest (ROIs) as nodes, and the edges represent the functional connectivity between these brain regions. We leverage pertinent node attributes to encapsulate the variability in brain activity corresponding to specific stimuli, serving as distinctive features for our classifier. This methodology enables us to unveil patterns and relationships in brain connectivity, offering enhanced insights into the complex dynamics of schizophrenia and the responses of individuals affected by it to auditory stimuli.

2. Literature Review

This section provides concise information about prior literature which has been consulted as reference during the model preparation. The application of graph based neural networks in the analysis of neural activity is an emerging area of study. Saeidi *et al* [1] have proposed an end-end GCN network on the benchmark HCP dataset, which makes use of statistical features extracted from the connectivity matrices as a node feature. Additionally, standard node embedding algorithms such as NetMF, RandNE, Node2Vec and Walklets were used to extract node features and their performance was analyzed. The paper acknowledges the importance of individual differences in brain function by testing the model on a gender-based and gF score-based sub-dataset. The effect of batch size was also accounted for. The proposed framework achieved an accuracy of 97.7% and concluded that NetMF and RandNE algorithms outperformed the rest.

Li, X. *et al* [2] have employed a custom framework BrainGNN, composed of Ra-GNN and R-pool blocks which are responsible for generating the node embeddings. The node embeddings are aggregated with its neighbors and the updated representations are projected onto a learnable vector which is fed to a classifier. The model was utilized on two distinct datasets: the Biopoint Autism Study Dataset (Biopoint) and the Human Connectome Project (HCP) 900 Subject Release [3]. The primary objective for the Biopoint dataset [4] was the classification of autism affected individuals and healthy controls. Conversely, for the HCP dataset, the focus was on classifying seven

cognitive and behavioral task states. BrainGNN demonstrates an enhancement in average accuracy ranging from 3% to 20% for autism classification. Additionally, it achieves an average accuracy of 93.4% for the classification on Human Connectome Project dataset.

3. Methodology

3.1. *fMRI dataset and preprocessing*

We obtained task fMRI data for 71 participants, 46 schizophrenic patients and 25 healthy controls subjected to three experimental conditions, word lists, sentence lists and reversed speech. White noise was the low-level control condition to which the task results were compared to. The schizophrenic patients are further classified into two classes, 23 subjects who experience auditory visual hallucinations (AVH+) and 23 subjects who do not (AVH-) (Table 1). The data was obtained using a 3T Philips Ingenia scanner employing a T2*-weighted echo-planar imaging (EPI) sequence. The acquisition consisted of 341 volumes, and the following parameters were applied: a repetition time (TR) of 2000ms, echo time (TE) of 30ms and a flip angle of 70°. The in-plane resolution was set to 3.5 × 3.5 mm, with a field of view (FOV) measuring 238 × 245 mm. The slice thickness was 3.5 mm, and an inter-slice gap of 0.75 mm was maintained. Slices, totaling 32 per volume, were acquired in an interleaved order parallel to the AC-PC plane [5]. Refer (Fig. 1.a) for raw data.

Table 1: Participants description

	HC N=25	SCHZ N=46	AVH+ N=23	AVH- N=23	Difference
Age	39.8 (14.08)	42.52 (10.72)	40.09 (12.97)	44.96 (7.38)	HC vs SCZ: t = -0.84, p = 0.404 AVH+ vs AVH-: t = -1.57, p = 0.127
Sex (M: F)|	18:7	36:10	20:3	16:7	HC vs SCZ: $\chi2$ = 0.35, p = 0.555 AVH+ vs AVH-: $\chi2$ = 2.04, p = 0.284
Current IQ (WAIS III)	108.00 (18.71)	95.44 (12.96)	92.09 (13.76)	99.32 (11.08)	HC vs SCZ: t = 2.76, p = 0.010 AVH+ vs AVH-: t = -1.83, p = 0.072
Duration of illness (years)	-	17.9 (10.40)	14.76 (10.57)	21.37 (9.26)	t = -2.11, p = 0.042
PSYRATS – Hallucination subscale	-	-	24.91 (7.32)	-	-

The preprocessing of the data was carried out using the FEAT module of FSL(FMRIB Software Library) [6]. The first 5 volumes were discarded to account for signal stabilization. Brain extraction was done using the BET tool. The functional data was then subjected to motion correction using the MCFLIRT algorithm and spatial smoothening (FWHM=5mm) was also applied (Fig 1.b) . FLIRT was used to register the low-resolution functional images to a high-resolution scan, and registration of the high-resolution scan to a standard MNI152) image. Using the transformation matrix obtained from the previous steps, we registered the functional sequence to the standard MNI space (Fig 1.c).

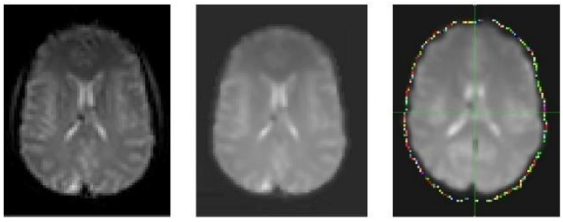

Fig 1 (a) depicts raw fMRI data. Fig 1 (b)- depicts fMRI data obtained after motion correction, brain extraction and smoothenting. Fig 1 (c) depicts the fMRI data post registration to MNI152 template

3.2. *Functional Graph Construction*

The preprocessed functional sequence underwent parcellation using the AAL atlas [7], dividing the brain into 116 Regions of Interest (ROI's). Based on the studies conducted by Soler-Vidal *et al* [5], the regions Left Superior Temporal Cortex, Occipital Cortex, Precuneus and Lingual Gyrus were found to exhibit a failure of deactivation in schizophrenic patients. The Left Superior Temporal Cortex is associated with language processing and speech comprehension. The Occipital Cortex and the Lingual Gyrus play a key role in visual processing, especially that of shapes and written words respectively. Precuneus is associated with elements of self-awareness and visuospatial processing. These regions are encompassed within the AAL atlas thereby was used for parcellation. The time points associated with specific activities were then extracted, and voxel information was collected. To derive the mean time series for each node, a bootstrapping technique was applied by randomly selecting one-fourth of the voxels within each ROI. This process is repeated ten times for augmentation.

The statistical features are obtained using the tsfresh algorithm (shown in Fig. 2), which integrates elements from hypothesis tests and feature significance testing [8]. Each feature vector produced undergoes a separate evaluation for its relevance to the specified target by utilizing p-values. The features derived from tsfresh encompass a comprehensive set of characteristics from both basic and advanced aspects of the time series.which are represented as "absolute_sum_of_changes,",

"benford_correlation", "variance," "standard deviation," "skewness,", "quantile", "count above mean", "count below mean", "longest strike above mean", "cubic complexity" and "complexity index" [1]. We make use of the Pearson correlation scores between the time series with all nodes contained in the graph. This helps encode information about the interconnectivity of the time series of each node that we have defined corresponding to these time points.

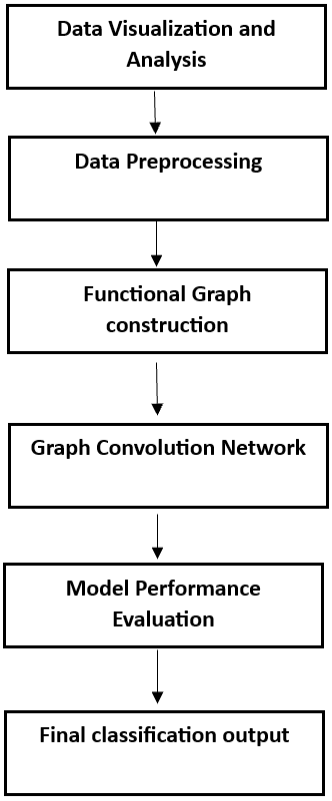

Fig. 2 Flowchart representation of methodology

3.3. *Model Architecture*

a) GraphSAGE:

The $GraphSAGE$ model [9] utilizes a sequence of three SAGE convolutional layers Eq. (1) to capture hierarchical representations from graph-structured data. Beginning with the extraction of node embeddings, each layer applies a SAGE convolution Eq. (1) followed by a ReLU activation. The model concludes with a readout layer, employing global mean pooling to aggregate node embeddings and produce a tensor summarizing graph-level information. A dropout layer with a probability of 0.5 mitigates overfitting during training. The final linear layer transforms the aggregated embeddings for classification into the specified number of classes.

$$h_v^{(l+1)} = \sigma\left(W_i \cdot CONCAT\left(h_v^{(l)}, AGGREGATE_k\left(\left\{h_u^{(l)}, \forall u \in N(v)\right\}\right)\right)\right) \quad (1)$$

$h_v^{(l)}$ denotes the node embedding for node v at layer l. W_l is the weight matrix for layer l. σ denotes the RELU activation function and CONCAT is the concatenation operation. (Fig 3.) denotes an overview of the model architecture.

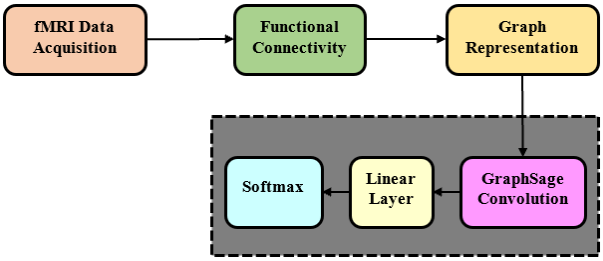

Fig. 3 Model architecture

b) GCN:

The proposed model architecture comprises three graph convolutional layers. To enhance stability and accelerate the training process, batch normalization is incorporated after each graph convolutional layer. Rectified Linear Unit (ReLU) activation functions follow each graph convolutional layer, introducing non-linearity to the model. Dropout regularization is systematically applied after each activation function during training to mitigate overfitting risks. Global mean pooling is incorporated to aggregate node representations across the entire graph. The model's learnable parameters are further transformed by a linear layer to project the aggregated node representations into the final output space. Lastly, the model outputs are subject to a SoftMax activation facilitating the derivation of class probabilities which is given in Eq. (2).

$$h_i^{(l+1)} = \sigma\left(\sum_{j \in N(i)} \frac{1}{c_{ij}} W^{(l)} h_j^{(l)}\right) \quad (2)$$

$h_v^{(l+1)}$ denotes the updated representation of node layer $(l+1)$. σ denotes the activation function. $\sum$ denotes the weighted sum function. $W^{(l)}$ is the weight matrix at layer l and $h_j^{(l)}$ is the feature representation of node j. The normalization term is denoted by c_{ij}.

3.4. *Training and Testing*

This study utilized an 80-10-10 split for training, validation, and test sets, respectively. The validation split was conducted on the training data. To augment the test data, one-fourth of the voxels from the Regions of Interest (ROIs) were randomly selected and bootstrapped ten times. In the training set, four subjects from the

healthy class (class 0) and three each from AVH- (class 1) and AVH+ (class 2) were included. This was done for two different experimental conditions namely "sentences" and "reversed". The model makes uses of Adam optimizer with a learning rate of 0.001.
Cross-Entropy Loss was chosen as the loss function as it is primarily used for multi-class classification.

3.5. *Model Evaluation*

Evaluation metrics are described from Eqs. (3), (4), (5), (6), (7) and (8) such as precision, recall, accuracy, balanced accuracy, F1-scores and MCC were used to assess the model's performance.

a) Precision: It denotes the extent to which a model accurately recognizes positive instances among all the instances it labeled as positive, highlighting its capability to reduce the occurrence of false positives.

$$Precision = \frac{TP}{TP + FP} \tag{3}$$

b) Recall: Recall is an assessment of a model's effectiveness in recognizing all positive instances among the entire set of actual positive instances. It showcases the model's capacity to reduce false negatives and encompass all pertinent outcomes.

$$Recall = \frac{TP}{TP + FN} \tag{4}$$

c) Accuracy: It signifies the gauge of the model's accuracy in correctly categorizing instances across all classes, providing insight into the overall correctness of its predictions.

$$Accuracy = \frac{TP + TN}{TP + FN + TN + FN} \tag{5}$$

d) Balanced Accuracy: Balanced Accuracy (BA) is a metric that considers class imbalances when assessing the overall correctness of a classification model by calculating the mean sensitivity across all classes.

$$BA = 0.5 * \left(\frac{TP}{TP + FN}\right) + \left(\frac{TN}{TN + FP}\right) \tag{6}$$

e) F1 Score: It evaluates the model's capacity to accurately recognize positive instances, taking into account both precision and recall

$$F1\ Score = \frac{2 * Precision * Recall}{Precision + Recall} \tag{7}$$

f) MCC (Matthew's Correlation Coefficient): Factors in true positives, true negatives, false positives, and false negatives, offering a well-balanced metric, particularly effective in situations where there is an imbalance between classes.

$$MCC = \frac{TP * TN - FP * FN}{\sqrt{(TP + FP)(TP + FN)(TN + FP)(TN + FN)}} \tag{8}$$

4. Result and Analysis

The $GraphSAGE$ model was trained using functional graphs corresponding to the 'sentences' and 'reversed' conditions. It achieved an accuracy of 97% after 20 epochs for the 'sentences' condition and a 95% accuracy after 20 epochs for the 'reversed' condition**. (**Table 2 and Table 3) summarizes the performance of this model.

Table 2: Evaluation metrics for GraphSAGE

Evaluation Metrics	SENTENCES	REVERSED
MCC	0.9570	0.9356
Accuracy (%)	97.18%	95.77%
F1 Micro (%)	97.18%	95.77%
F1 Macro (%)	96.94%	95.29%
F1 Weighted (%)	97.14%	95.92%
Bal. accuracy (%)	96.96%	95.92%
Precision	0.9718	0.9490
Recall score	0.9696	0.9592

Table 3: Evaluation metrics for GCN

Evaluation Metrics	SENTENCES	REVERSED
MCC	0.8955	0.7436
Accuracy (%)	92.95%	81.69%
F1 Micro (%)	92.95%	81.69%
F1 Macro (%)	93.02%	78.17%
F1 Weighted (%)	92.97%	81.30%
Bal. accuracy (%)	94.31%	78.18%
Precision	0.9232	0.8761
Recall score	0.9431	0.7818

Fig. 4(a) and 4(b) depict the changes in training and validation loss, as well as training and validation accuracy across different epochs for $GraphSAGE$ model with 'sentence' condition.

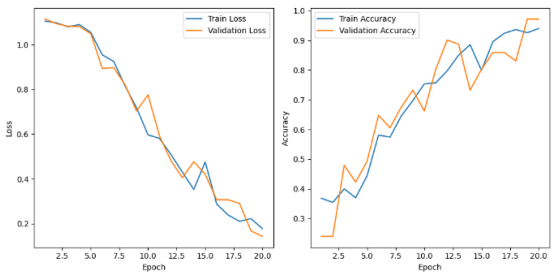

a) **b)**

Figure 4. GraphSAGE Training and validation a) Loss b)Accuracy- for stimulus 1.

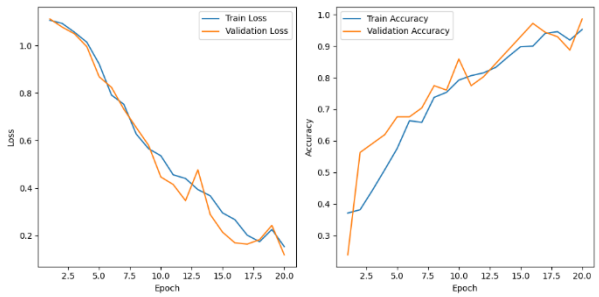

a) **b)**

Figure 5. GraphSAGE Training and validation a) Loss b) Accuracy- for stimulus 2

Fig 5(a) and 5(b) denote the changes in training and validation loss, as well as training and validation accuracy over epochs for $GraphSAGE$ model with 'reversed' condition.

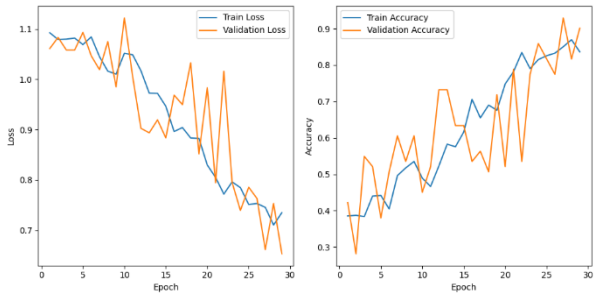

a) **b)**

Figure 6. GCN Training and validation a) Loss b)Accuracy- for stimulus 1

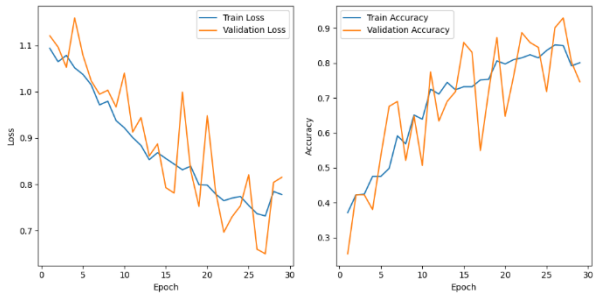

a) **b)**

Figure 7. GCN Training and validation a) Loss b) Accuracy- for stimulus 2

Fig. 6(a) and 6(b) depict the changes in training and validation loss, as well as training and validation accuracy across different epochs for $\boldsymbol{GCN}$ model with 'sentence' condition. Fig 7(a) and 7(b) denote the changes in training and validation loss, as well as training and validation accuracy over epochs for $\boldsymbol{GCN}$ model with 'reversed' condition.

The GCN model was trained using functional graphs corresponding to the 'sentences' and 'reversed' conditions. It achieved an accuracy of 92% after 30 epochs for the 'sentences' condition and 81% accuracy after 30 epochs for the 'reversed' condition**.** (Table 3) summarizes the performance of this model.

Figs 4, 5, 6, 7 summarizes the trends of training loss and accuracy vs validation loss and accuracy over the course of epochs. The decreasing trend over epochs with respect to training loss is indicative of effective model training. Concurrently, the validation loss which represents the model's performance on unseen data steadily decreases, signifying successful generalization.

The observed increasing trend in both training and validation accuracy plots suggests that the model is learning and generalizing effectively over epochs. The rising training accuracy indicates successful adaptation to the training data, while the parallel increase in validation accuracy implies robust generalization to unseen data. This positive trajectory signifies continuous improvement in the model's performance, showcasing its ability to capture underlying patterns in the data.

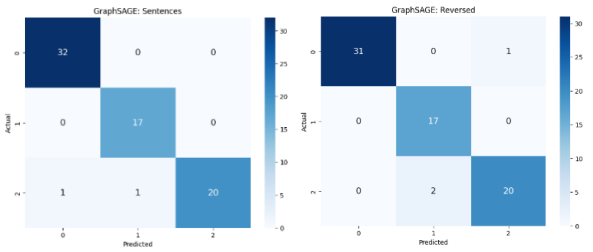

a) **b)**

Figure 8. Confusion Matrix of GraphSAGE for a) Stimulus 1 b) Stimulus 2.

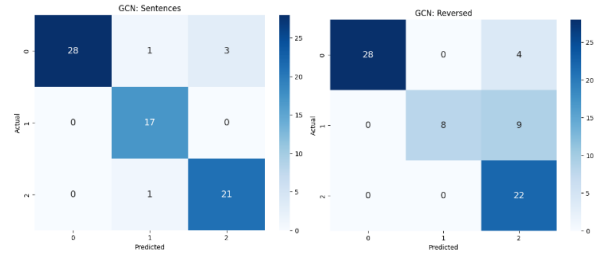

a) **b)**

Figure 9. Confusion Matrix of GCN for a) Stimulus 1 b) Stimulus 2.

Table 4: Comparative Results Analysis

	Sentences						Reversed					
	GraphSAGE			GCN			GraphSAGE			GCN		
Metrics	**HC**	**AVH-**	**AVH+**	**HC**	**AVH-**	**AVH+**	**HC**	**AVH-**	**AVH+**	**HC**	**AVH-**	**AVH+**
Accuracy	97%			93%			96%			82%		
Precision	0.97	0.94	1	1	0.89	0.88	1	0.89	0.95	1	1	0.63
Recall	1	1	0.91	0.88	1	0.95	0.97	1	0.91	0.88	0.47	1
F1-Score	98%	97%	95%	93%	94%	91%	98%	94%	93%	93%	64%	77%

The confusion matrix outlines true positives, true negatives, false positives, and false negatives, and is used to assess prediction accuracy. Fig 8.a and 8.b depict the confusion matrices of the $GraphSAGE$G model for both the sentences and reversed conditions respectively. Fig 9.a and 9.b represent the matrices of the $\boldsymbol{GCN}$ model for the sentences and reversed conditions respectively.

On comparison of the model metrics of $GraphSAGE$, the model exhibits proficiency in distinguishing between the 'sentences' and 'reversed' conditions. Notably, for 'sentences' performs better than 'reversed' across all metrics, refer (Table 2). These results underscore the model's discriminative capability, effectively capturing nuanced distinctions in functional graphs associated with the specified conditions. The overall performance is observed to be enhanced for the 'sentences' condition and this highlights the model's efficacy in this specific cognitive context.

The performance metrics for the 'sentences' and 'reversed' conditions for the GCN are summarized in (Table 3). The MCC, a measure considering true and false positives and negatives, is notably high for both conditions, indicating strong classification performance. The 'sentences' condition exhibits higher values across these metrics, suggesting enhanced classification ability for sentences stimuli. Overall, these metrics collectively affirm the effectiveness of the model in distinguishing between the specified conditions, with 'sentences' achieving significantly enhanced performance.

The comparative analysis for the two models is summarized in (Table 4). From the metrics, it can be inferred that $GraphSAGE$ performs better by achieving higher accuracy of 97% and 96% for both the conditions while the GCN model achieves an accuracy of 93% and 82% for sentences and reversed condition respectively. Between the given conditions, we can infer that the 'sentence' condition results in a better accuracy for both the models and can therefore be considered a more suitable distinguishing stimuli among the subjects.

5. Conclusion

Our study employs two different graph convolution-based architectures namely $GraphSAGE$ and $\boldsymbol{GCN}$. Both these architectures examine the distinctions in brain activity of 71 participants. The participant population consists of healthy controls, schizophrenic patients with hallucination (AVH+) and schizophrenic patients without hallucination (AVH-). These groups were subjected to three different auditory stimuli namely 'words', 'sentences' and 'reversed'. This analysis particularly focuses on the 'sentences' and 'reversed' stimulus on the participant group. Our study primarily focusses to identify the activation differences among the two stimuli.

The differences would be leveraged to classify among the three classes. The fMRI data was preprocessed and registered to the MNI152 template in order to bring it to a standard coordinate space. Parcellation was applied to the preprocessed data through the AAL atlas. This atlas contains regions such as Lingual Gyrus and Left temporal auditory cortex which play a primal role in visual processing and speech perception [10].

In the studies conducted by Soler-Vidal *et al* [5] on the dataset, it was concluded that out of the three conditions, included in the experiment, the sentences condition and the reversed condition together varied significantly from the words condition. Further the activation patterns observed for 'sentences' and 'reversed' stimuli did not show clear distinction. They also concluded that there was no appropriate distinguishing factor between the AVH+ and AVH- participants. Moreover, their studies have highlighted a reduced activation of the left primary auditory cortex when subjected to sentences and reversed speech. The auditory cortex plays a primal role in receiving and processing auditory information, including speech comprehension. A reduced activation of this region indicates disruptions in the neural pathways associated with auditory perception and interpretation [11][12].

Through our analysis we were able to find that the graph convolution-based $GraphSAGE$ model performs better than the GCN model. Further, our results suggest subtle distinctions within the AVH+ and AVH- classes, for both the conditions as well as effectively distinguishing

between healthy individuals and those with schizophrenia. We speculate that the minor differences among the sentences and reversed conditions could be used as a distinguishing factor among people with and without auditory-visual hallucinations. Our findings are in line with the results obtained by Soler-Vidal *et al* [5] and additionally we conclude that though the activation patterns for the 'sentences' and 'reversed' stimuli are similar, there are intricate differences which can be leveraged by our model to understand the effect of auditory-visual hallucination on schizophrenic patients.

The current study can be further extended to specific regions that show significant changes in the activation functions. These specific regions with the use of more complex graph-based architecture and larger group of subjects will provide notable insights in understanding the changes in auditory and speech perceptions among individuals affected with schizophrenia with ranging symptoms.

Acknowledgement

The first and second authors express their gratitude to Vellore Institute of Technology (VIT), Chennai, for providing valuable computational facilities and serving as a source of motivation. Additionally, they extend they're thanks to their respective faculties for unwavering support and guidance throughout the research endeavor.

References

1. Saeidi, M.; Karwowski, W.; Farahani, F.V.; Fiok, K.; Hancock, P.A.; Sawyer, B.D.; Christov-Moore, L.; Douglas, P.K. Decoding Task-Based fMRI Data with Graph Neural Networks, Considering Individual Differences. Brain Sci. 2022, 12, 1094. https://doi.org/10.3390/brainsci12081094
2. Li, X., Zhou, Y., Dvornek, N., Zhang, M., Gao, S., Zhuang, J., ... & Duncan, J. S. (2021). Braingnn: Interpretable brain graph neural network for fmri analysis. Medical Image Analysis, 74, 102233.
3. Van Essen, D.C., Smith, S.M., Barch, D.M., Behrens, T.E., Yacoub, E., Ugurbil, K., Consortium, W.M.H., et al.: The wu-minn human connectome project: anoverview. Neuroimage 80, 62–79 (2013)
4. Venkataraman, A., Yang, D.Y.J., Pelphrey, K.A., Duncan, J.S.: Bayesian community detection in the space of group-level functional differences. IEEE transactionson medical imaging 35(8), 1866–1882 (2016)
5. Joan Soler-Vidal and Paola Fuentes-Claramonte and Pilar Salgado-Pineda and Nuria Ramiro and María Ángeles García-León and María Llanos Torres and Antonio Arévalo and Amalia Guerrero-Pedraza and Josep Munuera and Salvador Sarró and Raymond Salvador and Wolfram Hinzen and Peter McKenna and Edith Pomarol-Clotet (2022). Brain correlates of speech perception in schizophrenia patients with and without auditory hallucinations. OpenNeuro. [Dataset] doi: doi:10.18112/openneuro.ds004302.v1.0.1
6. M.W. Woolrich, S. Jbabdi, B. Patenaude, M. Chappell, S. Makni, T. Behrens, C. Beckmann, M. Jenkinson, S.M. Smith. Bayesian analysis of neuroimaging data in FSL. NeuroImage, 45:S173-86, 200
7. Automated anatomical labelling atlas 3. Rolls, E. T., Huang, C. C., Lin, C. P., Feng, J., & Joliot, M., Neuroimage, 2020, 206, 116189, doi:10.1016/j.neuroimage.2019.116189
8. Christ, M.; Kempa-Liehr, A.W.; Feindt, M. Distributed and parallel time series feature extraction for industrial big data applications. *arXiv* **2016**, arXiv:1610.07717.
9. Veličković, Petar, et al. "Graph attention networks." arXiv preprint arXiv:1710.10903 (2017).
10. Shergill, S. S., et al. "SES04. 03 Auditory hallucinations: Mapping the neural network using functional magnetic resonance imaging." European Psychiatry 15.S2 (2000): 242s-242s.
11. Hamilton, Will, Zhitao Ying, and Jure Leskovec. "Inductive representation learning on large graphs." Advances in neural information processing systems 30 (2017).
12. Ford, Judith M., et al. "Tuning in to the voices: a multisite FMRI study of auditory hallucinations." Schizophrenia bulletin 35.1 (2009): 58-66. https://journals.plos.org/plosone/article?id=10.1371/journal.pone.0276975

Authors Introduction

Ms.Tejaswini Thota

She is currently pursuing his B.Tech degree in Computer Science with specialization in Artificial Intelligence and Robotics from School of Computer Science and Engineering, Vellore Institute of Technology, Chennai, India.

Mr. Reuben Stephen John

He is currently pursuing his B.Tech degree in Computer Science with specialization in Artificial Intelligence and Robotics from School of Computer Science and Engineering, Vellore Institute of Technology, Chennai, India.

Dr. Dhanush R.

Dr. Dhanush R is an Associate Professor in the School of Electronics Engineering, VIT Chennai. His research interests include Neuroscience, Biomechanics. Motor learning, Motor Control.

Dr. Amutha S

Dr. Amutha S is currently working as an Assistant Professor, School of Computer Science and Engineering, Vellore Institute of Technology, Chennai, India. Her area of research includes Data mining, Machine learning, Pattern detection, HCI, IoT/IoMT and Deep learning.

Dr. Heshalini Rajagopal

She received her PhD and Master's degree from the Department of Electrical Engineering, University of Malaya, Malaysia in 2021 and 2016 respectively. Her research interest includes image processing, artificial intelligence and machine learning